

Stability of Bogoliubov Fermi surfaces within BCS theory

Ankita Bhattacharya^{1,*} and Carsten Timm^{1,2,†}

¹*Institute of Theoretical Physics, Technische Universität Dresden, 01062 Dresden, Germany*

²*Würzburg-Dresden Cluster of Excellence ct.qmat, Technische Universität Dresden, 01062 Dresden, Germany*



(Received 2 February 2023; revised 24 May 2023; accepted 25 May 2023; published 5 June 2023)

It has recently been realized that the gap nodes of multiband superconductors that break time-reversal symmetry generically take the form of Fermi surfaces of Bogoliubov quasiparticles. However, these Fermi surfaces lead to a nonzero density of states (DOS) at the Fermi energy, which typically disfavors such superconducting states. It has thus not been clear whether they can be stable for reasonable pairing interactions or are in practice preempted by time-reversal-symmetric states with vanishing DOS. In this Letter, we show within BCS theory applied to a paradigmatic model that the time-reversal-symmetry-breaking states are indeed stabilized over broad parameter ranges at weak coupling. Moreover, we introduce a fast method that involves solving the inverse BCS gap equation, does not require iteration, does not suffer from convergence problems, and can handle metastable solutions.

DOI: [10.1103/PhysRevB.107.L220501](https://doi.org/10.1103/PhysRevB.107.L220501)

Introduction. Recent years have witnessed a surge of interest in multiband superconductors (MSCs). In many complex superconductors, multiple bands are close to or cross the Fermi energy [1–11]. The multiband structure arises from internal degrees of freedom beyond the electron spin, e.g., orbital or basis site. These internal degrees of freedom lead to much richer possibilities for the states of Cooper pairs and hence to superconducting properties that are qualitatively different from the single-band case [12–14]. Specifically, MSCs enable exotic “internally anisotropic” pairing states [14]—momentum-independent *s*-wave pairing can have a nontrivial dependence on lattice symmetries.

Moreover, research has been stimulated by the prediction that gap nodes in time-reversal-symmetry-breaking (TRSB) states of MSCs are generically inflated into two-dimensional Fermi surfaces of Bogoliubov quasiparticles [Bogoliubov Fermi surfaces (BFSs)] [12–20]. In single-band models or if interband pairing is neglected, the superconducting gap typically closes at points or lines in momentum space (point or line nodes, respectively) or is everywhere nonzero. BFSs can be viewed as such nodes that are inflated into surfaces by a pseudomagnetic field generated by interband pairing.

The presence of BFSs implies a nonzero DOS at the Fermi energy, which leads to characteristic signatures in, e.g., the specific heat, the penetration depth, and the spin-lattice relaxation rate [21]. MSCs that break time-reversal symmetry (TRS), and are thus potential test beds for the physics discussed here, include UPt_3 [22,23], UBe_{13} and $\text{U}_{1-x}\text{Th}_x\text{Be}_{13}$ [24], Sr_2RuO_4 [25–27], $\text{PrOs}_4\text{Sb}_{12}$ [28,29],

iron-based superconductors [30–32], half-Heusler compounds [33], and CeRh_2As_2 [34]. However, the nonzero DOS raises fundamental concerns: Can superconductors with BFSs be energetically stable at all? There are always competing pairing states that do not break TRS and at most have point or line nodes. In such states, electronic spectral weight is pushed away from the Fermi energy compared to superconductors with BFSs, which is expected to lower the free energy. Preliminary estimates in Ref. [13] and BCS results from Ref. [35], where the main interest was in the role of spin-orbit coupling, indicate that BFSs could be stable under realistic conditions. A recently suggested orbital-antisymmetric spin-triplet pairing state of Sr_2RuO_4 also features BFSs [10].

In this Letter, we study a prototypical model [13,14,36,37] of cubic superconductors describing electrons with an effective angular momentum $j = 3/2$ within BCS theory [38]. We restrict ourselves to local pairing. Nonlocal pairing allows for additional symmetries of pairing states but does not introduce fundamentally new aspects [18].

The standard approaches to obtain the pairing amplitudes within BCS theory are to either solve the gap equation self-consistently or to minimize the free energy. These methods are computationally expensive since they require iteration, and they may fail to converge. We adopt a different strategy, namely to solve the *inverse gap equation*, which avoids these problems. We find that TRSB states with BFSs are indeed favored over broad parameter ranges for not too strong pairing interactions.

Model. We consider an effective spin-3/2 model with point group O_h [13,14,36,37]. The Hilbert space of internal degrees of freedom is thus four dimensional. The effective spin 3/2 emerges due to the presence of strong spin-orbit coupling and provides the natural description of electrons close to a fourfold Γ_8^+ ($F_{3/2,g}$) band-touching point. The concept of BFSs is not limited to $j = 3/2$ systems; the multiband nature may also arise due to other internal degrees of freedom [14,18].

*ankita.bhattacharya@tu-dresden.de

†carsten.timm@tu-dresden.de

We expand the normal-state Hamiltonian into a basis of Hermitian 4×4 matrices h_n as

$$H_N(\mathbf{k}) = \sum_{n=0}^5 c_n(\mathbf{k}) h_n. \quad (1)$$

The functions $c_n(\mathbf{k})$ are periodic basis functions of irreducible representations (irreps) of O_h that transform in the same way as the corresponding matrices h_n so that $H_N(\mathbf{k})$ is invariant under O_h . The matrices h_n can be chosen such that h_1, \dots, h_5 anticommute pairwise and h_0 , the 4×4 identity matrix, commutes with any matrix [18]. The basis matrices h_n and the functions $c_n(\mathbf{k})$ are listed in the Supplemental Material (SM) [39]. The normal-state eigenenergies are $\xi_{\mathbf{k}\pm} = c_0(\mathbf{k}) \pm \sqrt{c_1^2(\mathbf{k}) + \dots + c_5^2(\mathbf{k})}$.

Even-parity local pairing allows for six possible pairing channels, which belong to the one-dimensional irrep A_{1g} , the two-dimensional irrep E_g , and the three-dimensional irrep T_{2g} [13,14,37]. After mean-field decoupling, the pairing interaction reads as [13,14,36]

$$H_{\text{BCS}}^{\text{int}} = \frac{1}{2} \sum_{\mathbf{k}} \sum_{n=0}^5 [\Delta_n^* c_{-\mathbf{k}}^T (h_n U_T)^\dagger c_{\mathbf{k}} + \Delta_n c_{\mathbf{k}}^\dagger h_n U_T c_{-\mathbf{k}}^\dagger] + \frac{N}{2} \sum_{n=0}^5 \frac{|\Delta_n|^2}{V_n}. \quad (2)$$

Here, N is the number of unit cells, and for attractive pairing interactions we take $V_n > 0$. The pairing amplitudes are given by

$$\Delta_n \equiv \Delta_n^1 + i\Delta_n^2 = -\frac{V_n}{N} \sum_{\mathbf{k}} \langle c_{-\mathbf{k}}^T (h_n U_T)^\dagger c_{\mathbf{k}} \rangle, \quad (3)$$

where $U_T = \exp(iJ_y \pi)$ is the unitary part of the time-reversal operator. Neglecting an irrelevant constant, the full BCS Hamiltonian can then be written as

$$H_{\text{BCS}} = \frac{1}{2} \sum_{\mathbf{k}} \Psi_{\mathbf{k}}^\dagger \mathcal{H}(\mathbf{k}) \Psi_{\mathbf{k}} + \frac{N}{2} \sum_{n=0}^5 \frac{|\Delta_n|^2}{V_n} \quad (4)$$

in terms of the Nambu spinor $\Psi_{\mathbf{k}} = (c_{\mathbf{k}}, c_{-\mathbf{k}}^\dagger)^T$ and the Bogoliubov–de Gennes (BdG) Hamiltonian

$$\mathcal{H}(\mathbf{k}) = \begin{pmatrix} H_N(\mathbf{k}) & \hat{\Delta} \\ \hat{\Delta}^\dagger & -H_N^T(-\mathbf{k}) \end{pmatrix}, \quad (5)$$

where $\hat{\Delta} = \sum_{n=0}^5 (\Delta_n^1 + i\Delta_n^2) h_n U_T$.

Inverse gap equation. The free energy per unit cell resulting from H_{BCS} reads as [10,45]

$$F = -\frac{k_B T}{2N} \sum_{\mathbf{k}} \sum_{i=1}^8 \ln(1 + e^{-\beta E_{\mathbf{k},i}}) + \frac{1}{2} \sum_{n=0}^5 \sum_{\alpha=1}^2 \frac{(\Delta_n^\alpha)^2}{V_n^\alpha}, \quad (6)$$

where $E_{\mathbf{k},i}$ are the eigenvalues of the BdG Hamiltonian, i denotes the band, and $\beta = 1/k_B T$ is the inverse temperature. $E_{\mathbf{k},i}$ can be obtained in closed form, as discussed in the SM [39]. We temporarily allow the interaction strength V_n^α to depend on the index α referring to the real and imaginary parts of the pairing amplitudes.

Equating the derivative of the free energy with respect to Δ_n^α to zero, we obtain the BCS gap equation

$$\Delta_n^\alpha = \frac{V_n^\alpha}{2N} \sum_{\mathbf{k}} \sum_{i=1}^4 \tanh \frac{\beta E_{\mathbf{k},i}}{2} \frac{\partial E_{\mathbf{k},i}}{\partial \Delta_n^\alpha} \equiv V_n^\alpha f_n^\alpha(\Delta), \quad (7)$$

where we have used that the spectrum at fixed \mathbf{k} is symmetric. $\Delta \equiv (\Delta_0^1, \dots, \Delta_5^1; \Delta_0^2, \dots, \Delta_5^2) \in \mathbb{R}^{12}$ is the vector of all order parameters. $f_n^\alpha(\Delta)$ has to be of at least first order in Δ_n^α since otherwise the normal-state solution $\Delta = \mathbf{0}$ would not exist [39]. Hence, we can write $f_n^\alpha(\Delta) \equiv \Delta_n^\alpha g_n^\alpha(\Delta)$. For $\Delta_n^\alpha \neq 0$, solving Eq. (7) for V_n^α yields the inverse gap equation

$$V_n^\alpha = \frac{1}{g_n^\alpha(\Delta)}. \quad (8)$$

This equation describes the interaction strength that is necessary to obtain a given Δ . If $g_n^\alpha(\Delta)$ vanishes and V_n^α thus diverges the given Δ cannot be stabilized by any value of the interaction. On the other hand, for $\Delta_n^\alpha = 0$, Eq. (7) becomes tautological ($0 = 0$) and there is no constraint on V_n^α —a state without pairing in the Δ_n^α channel is compatible with any value of V_n^α (the state might not be the global minimum, though).

We first discuss the case without any symmetries. In this case, the parameter space is spanned by $6 \times 2 = 12$ independent coupling constants V_n^α . In principle, one can scan the 12-component order parameter Δ over the relevant ranges and obtain the 12 coupling constants $\mathbf{V} \equiv (V_0^1, \dots, V_5^1; V_0^2, \dots, V_5^2)$ from Eq. (8). Then the mapping is inverted to obtain $\mathbf{V} \mapsto \Delta$. This is generically possible at least locally since its domain and codomain have the same dimension. If there are multiple solutions for a \mathbf{V} , then the solution with the minimum free energy is stable.

If s order parameters Δ_n^α vanish, this corresponds to a $(12 - s)$ -dimensional subspace of the space of Δ . The inverse gap equations map this subspace into a codomain of generically the same dimension $12 - s$. The s coupling constants belonging to the vanishing Δ_n^α are arbitrary. Hence, restricting any number of order parameters to zero does not reduce the dimension of the space of allowed coupling constants. Indeed, in the normal state, all Δ_n^α vanish and all V_n^α are unconstrained.

Symmetries reduce the number of independent coupling constants. Due to the global $U(1)$ symmetry, V_n^α does not depend on α and we thus drop the superscript again. The presence of cubic symmetry further restricts the number of independent V_n . For local pairing, the six components of the pairing matrix $\hat{\Delta}$ transform according to the three irreps A_{1g} , T_{2g} , and E_g [14,18,36]. The coupling constants belonging to the same irrep must be equal. Hence, we can organize them as

$$A_{1g} : V_A \equiv V_0, \quad (9)$$

$$T_{2g} : V_T \equiv V_1 = V_2 = V_3, \quad (10)$$

$$E_g : V_E \equiv V_4 = V_5. \quad (11)$$

Note that the inverse gap equations still generically map the 12-dimensional space of Δ onto a 12-dimensional image of couplings \mathbf{V} but now only a three-dimensional submanifold is allowed. Random points Δ map onto unphysical \mathbf{V} with probability one. We thus need to restrict the values of Δ . Landau theory is very helpful to identify likely relations between

amplitudes Δ_n^α belonging to the same irrep [14,36,46]. For example, the only fundamentally different patterns of pairing amplitudes expected for the E_g channels are $(\Delta_4, \Delta_5) \propto (1, 0)$, $(0, 1)$, and $(1, i)$.

For pure-irrep pairing, the Δ_n^α belonging to all but one irrep vanish. The couplings V_n for all but this single irrep are then unconstrained. We solve the inverse gap equation for each of the expected patterns of pairing amplitudes for this irrep. These are one-to-one mappings and thus easy to invert. Mixed-irrep pairing states can also be treated: Let there be n_Γ irreps with nonzero pairing. Free-energy arguments provide a set of plausible patterns, now depending on n_Γ independent amplitudes, one for each irrep involved. The inverse gap equation provides an n_Γ -to- n_Γ mapping from pairing amplitudes to couplings, which can generically be inverted. The free energy of the resulting pure-irrep and mixed-irrep solutions has to be compared to find the stable state.

The main advantages of the inverse gap equation are that it does not require iteration to reach self-consistency and thus avoids convergence problems and is much faster. Moreover, it easily deals with metastable and unstable branches in the vicinity of first-order phase transitions.

We emphasize that high precision in the integration over momentum space is essential for reaching the weak-coupling regime. This is numerically difficult because the weak-coupling behavior relies on a term proportional to $\Delta^2 \ln(\Delta/\Lambda)$ in the free (internal) energy at $T = 0$, which has to be separated from a Δ^2 contribution. We observe that summing over a momentum-space mesh becomes forbiddingly slow for three-dimensional systems. Instead, we have obtained good results using adaptive integration. Details are discussed in the SM [39]. The high precision required for the three-dimensional momentum integration makes iterative methods prohibitively costly.

Results. In this Letter, we restrict ourselves to zero temperature. We first discuss E_g pairing states, which are described by the two-component order parameter $(\Delta_4, \Delta_5) \equiv \Delta (\delta_{x^2-y^2}, \delta_{3z^2-r^2}) \equiv \Delta \delta$ [14]. The pairing matrix reads as

$$\hat{\Delta} = \Delta (\delta_{x^2-y^2} h_4 U_T + \delta_{3z^2-r^2} h_5 U_T), \quad (12)$$

where the basis matrices h_4 and h_5 transform as $x^2 - y^2$ and $3z^2 - r^2$, respectively, under O_h [39]. As noted above, potentially stable pairing states are the time-reversal-symmetric states with the patterns $\delta = (1, 0)$ and $(0, 1)$ and the TRSB state with $\delta = (1, i)/\sqrt{2}$ [14,36].

Figure 1(a) shows the pairing amplitudes Δ as functions of the coupling strength V_E for the three δ . At weak coupling, $\Delta(V_E)$ shows the expected weak-coupling scaling $\ln \Delta \sim A - B/V_E$ with constants A, B [39]. For large coupling strength, Δ exhibits a pronounced S shape, which is characteristic of a first-order phase transition. Correspondingly, the free-energy differences between superconducting and normal states, $\Delta F \equiv F_s - F_n$, exhibit a swallowtail feature as a function of V_E , as shown in Fig. 1(b). A similar self-crossing of the free energy was observed for superconducting states with finite-momentum Cooper pairs by Fulde and Ferrell [47], where the control parameter was an exchange field.

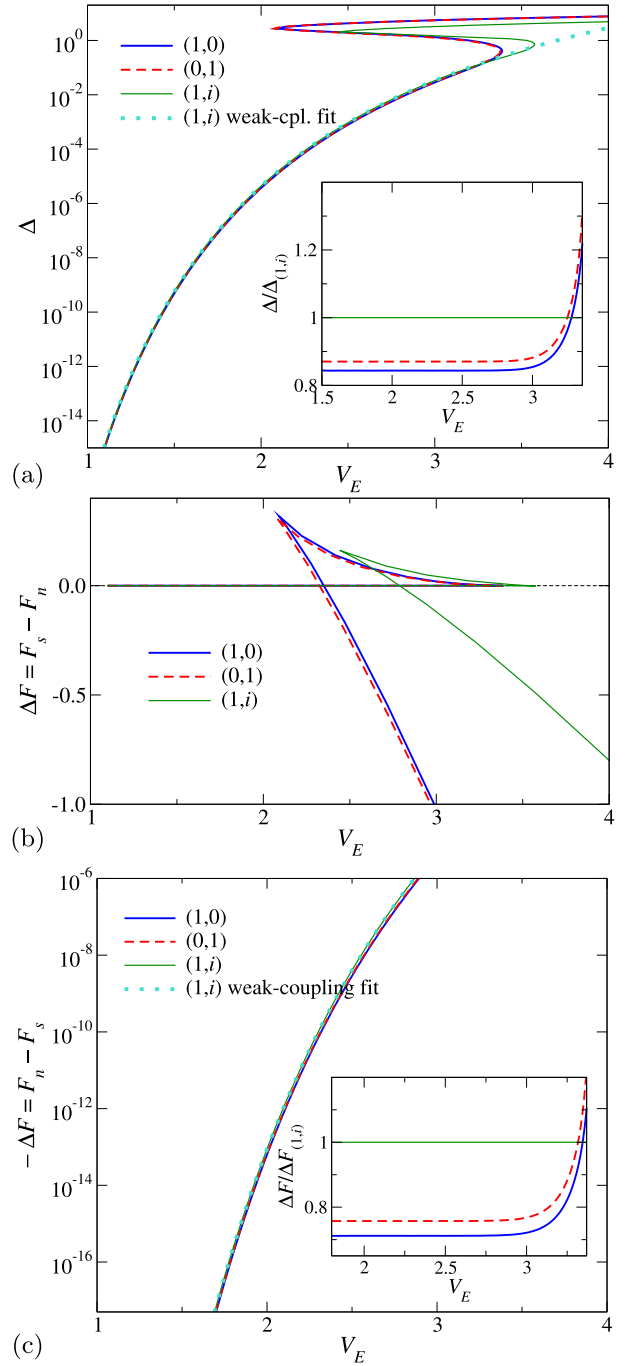


FIG. 1. (a) Pairing amplitudes Δ as functions of the coupling strength V_E at $T = 0$ for the E_g pairing states $(1, 0)$, $(0, 1)$, and $(1, i)$. At small V_E , $\Delta(V_E)$ shows weak-coupling scaling, $\ln \Delta \sim A - B/V_E$. The dotted curve is a fit of this scaling form to the numerical results for the $(1, i)$ state at small V_E . The inset shows the ratios of Δ for the three states to Δ for the $(1, i)$ state. (b) Free-energy differences $\Delta F = F_s - F_n$ between the superconducting and normal states as functions of the coupling strength V_E at $T = 0$. The state with minimal (most negative) ΔF is stable. (c) The same on a logarithmic scale, for the weak-coupling branches. Note that $-\Delta F > 0$ is plotted. At small V_E , we observe the weak-coupling scaling $\ln(-\Delta F) \sim A' - B'/V_E$. The dotted curve shows the weak-coupling scaling function for ΔF obtained from the fit in (a). The inset shows the ratios of ΔF for the three states to ΔF for the $(1, i)$ state. Numerical parameters are given in the SM [39].

In the range of V_E with three solutions, the one with the intermediate value of Δ and the highest value of the free energy corresponds to a maximum separating two (meta)stable states. The **S** shape thus means that for increasing coupling strength a second solution with a much larger pairing amplitude Δ appears, which initially is metastable. This solution can be attributed to interband pairing: The values of Δ for this branch are comparable to the energy difference between the normal-state bands. Hence, the superconducting pairing can take advantage of the additional DOS in these bands.

If there were a single E_g pairing state our results would predict a first-order transition without a change in symmetry similar to a liquid-gas transition. However, there are three distinct pairing states controlled by the same V_E . For weak coupling, the TRSB $(1, i)$ state is favored [see the inset in Fig. 1(c)]. Note that the favored state corresponds to the highest value since $\Delta F_{(1,i)} < 0$. However, at strong coupling, the $(1, i)$ state becomes strongly disfavored and there is a small preference for the $(0,1)$ state over the $(1,0)$ state. The $(1,0)$ state has two crossing line nodes ($x^2 - y^2$ symmetry) [37], which leads to a higher DOS close to the Fermi energy and is thus energetically unfavorable [46], compared to the $(0,1)$ state with noncrossing line nodes ($3z^2 - r^2$ symmetry).

Figure 1(c) shows the free-energy gain on a logarithmic scale at weak coupling. The free-energy gain follows the expected behavior $\ln(-\Delta F) \sim A' - B'/V_E$, where the parameters are not free but determined by the scaling form of Δ [39]. We again see that the TRSB state is favored in the weak-coupling limit. The inset in Fig. 1(c) shows that the energy separation between the three states is sizable on the relevant energy scale. We emphasize that the smaller values of Δ and ΔF shown in Fig. 1 would be experimentally out of reach. The main reason for plotting them here is to test the solution of the BCS gap equation—the numerical method remains viable deep into the weak-coupling regime.

The weak-coupling results can be understood following Ref. [46] since the TRSB $(1, i)$ state has point nodes in the limit of small V_E and thus has a lower DOS close to the Fermi energy than the $(1,0)$ and $(0,1)$ states, which have line nodes. With increasing coupling V_E , the point nodes are inflated into BFSs, which have larger DOS and are disfavored. The line nodes of the time-reversal-symmetric states are not inflated. Thus, at strong coupling, the TRSB state is destabilized.

We briefly comment on the T_{2g} pairing states. Similar to E_g pairing, we find a first-order transition from a TRSB state at weak coupling to the time-reversal-symmetric state at strong coupling. Details are shown in the SM [39].

So far, we have discussed pairing states that belong to a single irrep. However, mixed-irrep pairing states are possible when two pure-irrep states are nearly degenerate. We consider the mixed-irrep state $\Delta_{xy}^{T_{2g}} + i\Delta_{x^2-y^2}^{E_g}$, where the subscript describes the symmetry of the order parameter. This pairing state has only two point nodes in the limit $\Delta \rightarrow 0$ [37] and should thus be favored over all other mixed-irrep states, which have line nodes or more point nodes. We compare the free-energy gain as a function of the couplings V_E and V_T for this state to the pure E_g state with $\delta = (1, i)/\sqrt{2}$ and the pure T_{2g} state with $\delta = (1, i, 0)/\sqrt{2}$ in the weak-coupling regime in Fig. 2. As discussed above, the result for the pure E_g state does not

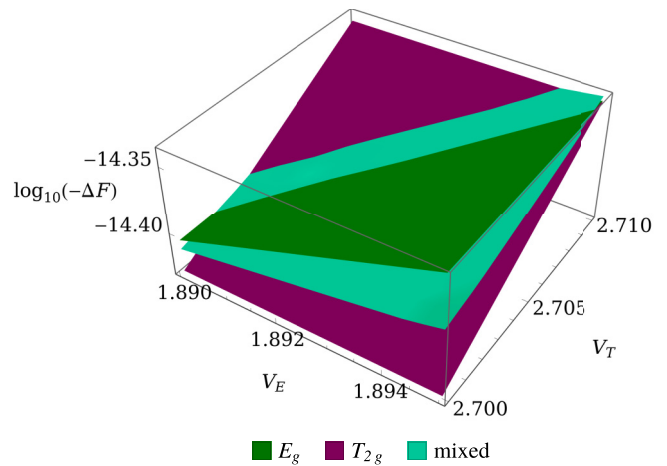


FIG. 2. Free-energy differences $\Delta F = F_s - F_n$ between the superconducting and normal states as functions of the coupling strengths V_E and V_T . A pure E_g state, a pure T_{2g} state, and a mixed-irrep state are compared (see text). Note that $-\Delta F > 0$ is plotted on a logarithmic scale so that the largest value corresponds to the stable state.

depend on the interaction in the T_{2g} channel and vice versa. We find that the mixed-irrep state is stabilized in a narrow region of coupling constants. This result is reasonable since the mixed-irrep state with two (inflated) point nodes is energetically favored over the E_g state with eight point nodes and the T_{2g} state with two point nodes and one line node [14] if the couplings are fine tuned close to degeneracy.

Conclusions. We have performed a BCS study of a paradigmatic centrosymmetric spin-3/2 model to analyze the stability of TRSB superconducting states with BFSs. At weak coupling, such TRSB states are indeed stable. For increasing pairing interactions, TRSB states become disfavored compared to time-reversal-symmetric states due to the increasing DOS at the Fermi energy resulting from the growing BFSs. This eventually leads to a first-order transition to a time-reversal-symmetric state at strong coupling. If there were only a single possible pairing state, our results would predict a liquid-gas-like first-order transition without a change in symmetry.

We have proposed an alternative approach to solve the BCS gap equations. The main idea is to solve the inverse equations to obtain the coupling strengths as functions of the pairing amplitudes and to invert the resulting mapping. If there is only a single coupling and a single amplitude, this inversion is a trivial interchange of axes but the method works beyond this case. The inverse gap equation avoids iterations and the associated convergence problems. It can also treat metastable and unstable branches as well as the resulting first-order transitions, which is essential for this work.

The approach has been derived for general temperatures and illustrated for the limit $T \rightarrow 0$. The application at $T > 0$ should in fact be numerically more benign since the weak-coupling scaling is cut off by T . The interesting questions of the relative stability of states with and without BFSs at $T > 0$ and the fate of the metastable solutions are left for future work.

Acknowledgments. The authors thank Philip M. R. Brydon and Julia M. Link for useful discussions. Financial support by the Deutsche Forschungsgemeinschaft, in part through

Collaborative Research Center SFB 1143, project A04, Project Id 247310070, and the Würzburg-Dresden Cluster of Excellence ct.qmat, EXC 2147, Project Id 390858490, is gratefully acknowledged.

-
- [1] Y. Gao, W.-P. Su, and J.-X. Zhu, Interorbital pairing and its physical consequences for iron pnictide superconductors, *Phys. Rev. B* **81**, 104504 (2010).
- [2] A. Nicholson, W. Ge, J. Riera, M. Daghofer, A. Moreo, and E. Dagotto, Pairing symmetries of a hole-doped extended two-orbital model for the pnictides, *Phys. Rev. B* **85**, 024532 (2012).
- [3] R. Nourafkan, G. Kotliar, and A.-M. S. Tremblay, Correlation-Enhanced Odd-Parity Interorbital Singlet Pairing in the Iron-Pnictide Superconductor LiFeAs, *Phys. Rev. Lett.* **117**, 137001 (2016).
- [4] T. Ong, P. Coleman, and J. Schmalian, Concealed d -wave pairs in the s^{\pm} condensate of iron-based superconductors, *Proc. Natl. Acad. Sci. USA* **113**, 5486 (2016).
- [5] E. M. Nica, R. Yu, and Q. Si, Orbital-selective pairing and superconductivity in iron selenides, *npj Quantum Mater.* **2**, 24 (2017).
- [6] A. V. Chubukov, O. Vafek, and R. M. Fernandes, Displacement and annihilation of Dirac gap nodes in d -wave iron-based superconductors, *Phys. Rev. B* **94**, 174518 (2016).
- [7] D. F. Agterberg, T. Shishidou, J. O'Halloran, P. M. R. Brydon, and M. Weinert, Resilient Nodeless d -Wave Superconductivity in Monolayer FeSe, *Phys. Rev. Lett.* **119**, 267001 (2017).
- [8] N. Kristoffel, P. Rubin, and T. Örd, Multiband superconductivity of doped cuprates, *J. Phys.: Conf. Ser.* **108**, 012034 (2008).
- [9] Y. Maeno, H. Hashimoto, K. Yoshida, S. Nishizaki, T. Fujita, J. G. Bednorz, and F. Lichtenberg, Superconductivity in a layered perovskite without copper, *Nature (London)* **372**, 532 (1994).
- [10] H. G. Suh, H. Menke, P. M. R. Brydon, C. Timm, A. Ramires, and D. F. Agterberg, Stabilizing even-parity chiral superconductivity in Sr₂RuO₄, *Phys. Rev. Res.* **2**, 032023(R) (2020).
- [11] G. E. Volovik and L. P. Gor'kov, Superconducting classes in heavy-fermion systems, *Zh. Eksp. Teor. Fiz.* **88**, 1412 (1985) [*Sov. Phys. JETP* **61**, 843 (1985)].
- [12] G. E. Volovik, Nonzero state density in superconductors with a high transition temperature, *Pis'ma Zh. Teor. Fiz.* **49**, 685 (1989) [*JETP Lett.* **49**, 790 (1989)]; Zeroes in the energy gap in superconductors with high transition temperature, *Phys. Lett. A* **142**, 282 (1989).
- [13] D. F. Agterberg, P. M. R. Brydon, and C. Timm, Bogoliubov Fermi Surfaces in Superconductors with Broken Time-Reversal Symmetry, *Phys. Rev. Lett.* **118**, 127001 (2017).
- [14] P. M. R. Brydon, D. F. Agterberg, H. Menke, and C. Timm, Bogoliubov Fermi surfaces: General theory, magnetic order, and topology, *Phys. Rev. B* **98**, 224509 (2018).
- [15] J. M. Link and I. F. Herbut, Bogoliubov Fermi Surfaces in Noncentrosymmetric Multicomponent Superconductors, *Phys. Rev. Lett.* **125**, 237004 (2020).
- [16] J. M. Link, I. Boettcher, and I. F. Herbut, d -wave superconductivity and Bogoliubov Fermi surfaces in Rarita-Schwinger-Weyl semimetals, *Phys. Rev. B* **101**, 184503 (2020).
- [17] S. Ono and K. Shiozaki, Symmetry-Based Approach to Superconducting Nodes: Unification of Compatibility Conditions and Gapless Point Classifications, *Phys. Rev. X* **12**, 011021 (2022).
- [18] C. Timm and A. Bhattacharya, Symmetry, nodal structures, and Bogoliubov Fermi surfaces for nonlocal pairing, *Phys. Rev. B* **104**, 094529 (2021).
- [19] P. Dutta, F. Parhizgar, and A. M. Black-Schaffer, Superconductivity in spin-3/2 systems: Symmetry classification, odd-frequency pairs, and Bogoliubov Fermi surfaces, *Phys. Rev. Res.* **3**, 033255 (2021).
- [20] D. Kim, S. Kobayashi, and Y. Asano, Quasiparticle on Bogoliubov Fermi surface and odd-frequency Cooper pair, *J. Phys. Soc. Jpn.* **90**, 104708 (2021).
- [21] C. J. Lapp, G. Börner, and C. Timm, Experimental consequences of Bogoliubov Fermi surfaces, *Phys. Rev. B* **101**, 024505 (2020).
- [22] E. R. Schemm, W. J. Gannon, C. M. Wishne, W. P. Halperin, and A. Kapitulnik, Observation of broken time-reversal symmetry in the heavy-fermion superconductor UPt₃, *Science* **345**, 190 (2014).
- [23] G. M. Luke, A. Keren, L. P. Le, W. D. Wu, Y. J. Uemura, D. A. Bonn, L. Taillefer, and J. D. Garrett, Muon Spin Relaxation in UPt₃, *Phys. Rev. Lett.* **71**, 1466 (1993).
- [24] G. R. Stewart, UBe₁₃ and U_{1-x}Th_xBe₁₃: Unconventional superconductors, *J. Low Temp. Phys.* **195**, 1 (2019).
- [25] G. M. Luke, Y. Fudamoto, K. M. Kojima, M. I. Larkin, J. Merrin, B. Nachumi, Y. J. Uemura, Y. Maeno, Z. Q. Mao, Y. Mori, H. Nakamura, and M. Sigrist, Time-reversal symmetry breaking superconductivity in Sr₂RuO₄, *Nature (London)* **394**, 558 (1998).
- [26] J. Xia, Y. Maeno, P. T. Beyersdorf, M. M. Fejer, and A. Kapitulnik, High Resolution Polar Kerr Effect Measurements of Sr₂RuO₄: Evidence for Broken Time-Reversal Symmetry in the Superconducting State, *Phys. Rev. Lett.* **97**, 167002 (2006).
- [27] V. Grinenko, S. Ghosh, R. Sarkar, J.-C. Orain, A. Nikitin, M. Elender, D. Das, Z. Guguchia, F. Brückner, M. E. Barber, J. Park, N. Kikugawa, D. A. Sokolov, J. S. Bobowski, T. Miyoshi, Y. Maeno, A. P. Mackenzie, H. Luetkens, C. W. Hicks, and H.-H. Klauss, Split superconducting and time-reversal symmetry-breaking transitions in Sr₂RuO₄ under stress, *Nat. Phys.* **17**, 748 (2021).
- [28] Y. Aoki, A. Tsuchiya, T. Kanayama, S. R. Saha, H. Sugawara, and H. Sato, Time-Reversal Symmetry-Breaking Superconductivity in Heavy-Fermion PrOs₄Sb₁₂ Detected by Muon-Spin Relaxation, *Phys. Rev. Lett.* **91**, 067003 (2003).
- [29] D. E. MacLaughlin, L. Shu, R. H. Heffner, J. E. Sonier, F. D. Callaghan, G. D. Morris, O. O. Bernal, W. M. Yuhasz, N. A. Frederick, and M. B. Maple, Multiband superconductivity and penetration depth in PrOs₄Sb₁₂, *Phys. B: Condens. Matter* **403**, 1132 (2008).
- [30] H. Hosono and K. Kuroki, Iron-based superconductors: Current status of materials and pairing mechanism, *Physica C* **514**, 399 (2015).
- [31] P. Bourgeois-Hope, S. Chi, D. A. Bonn, R. Liang, W. N. Hardy, T. Wolf, C. Meingast, N. Doiron-Leyraud, and L. Taillefer, Thermal Conductivity of the Iron-Based Superconductor FeSe:

- Nodeless Gap with a Strong Two-Band Character, *Phys. Rev. Lett.* **117**, 097003 (2016).
- [32] V. Grinenko, D. Weston, F. Caglieris, C. Wuttke, C. Hess, T. Gottschall, I. Maccari, D. Gorbunov, S. Zherlitsyn, J. Wosnitzer, A. Rydh, K. Kihou, C.-H. Lee, R. Sarkar, S. Dengre, J. Garaud, A. Charnukha, R. Hühne, K. Nielsch, B. Büchner, H.-H. Klauss *et al.*, State with spontaneously broken time-reversal symmetry above the superconducting phase transition, *Nat. Phys.* **17**, 1254 (2021).
- [33] H. Kim, K. Wang, Y. Nakajima, R. Hu, S. Ziemak, P. Syers, L. Wang, H. Hodovanets, J. D. Denlinger, P. M. R. Brydon, D. F. Agterberg, M. A. Tanatar, R. Prozorov, and J. Paglione, Beyond triplet: Unconventional superconductivity in a spin-3/2 topological semimetal, *Sci. Adv.* **4**, eaao4513 (2018).
- [34] M. Kibune, S. Kitagawa, K. Kinjo, S. Ogata, M. Manago, T. Taniguchi, K. Ishida, M. Brando, E. Hassinger, H. Rosner, C. Geibel, and S. Khim, Observation of Antiferromagnetic Order as Odd-Parity Multipoles inside the Superconducting Phase in CeRh₂As₂, *Phys. Rev. Lett.* **128**, 057002 (2022).
- [35] H. Menke, C. Timm, and P. M. R. Brydon, Bogoliubov Fermi surfaces stabilized by spin-orbit coupling, *Phys. Rev. B* **100**, 224505 (2019).
- [36] P. M. R. Brydon, L. M. Wang, M. Weinert, and D. F. Agterberg, Pairing of $j = 3/2$ Fermions in Half-Heusler Superconductors, *Phys. Rev. Lett.* **116**, 177001 (2016).
- [37] B. Roy, S. A. A. Ghorashi, M. S. Foster, and A. H. Nevidomskyy, Topological superconductivity of spin-3/2 carriers in a three-dimensional doped Luttinger semimetal, *Phys. Rev. B* **99**, 054505 (2019).
- [38] L. N. Cooper, Bound electron pairs in a degenerate fermi gas, *Phys. Rev.* **104**, 1189 (1956); J. Bardeen, L. N. Cooper, and J. R. Schrieffer, Microscopic theory of superconductivity, *ibid.* **106**, 162 (1957); Theory of superconductivity, *ibid.* **108**, 1175 (1957).
- [39] See Supplemental Material at <http://link.aps.org/supplemental/10.1103/PhysRevB.107.L220501> for details of the model, the parameter values used for the numerical calculations, analytical expressions for the quasiparticle energies, the derivation of weak-coupling scaling forms, details on the numerical integration, and results for T_{2g} pairing, which includes Refs. [40–44].
- [40] L. Savary, J. Ruhman, J. W. F. Venderbos, L. Fu, and P. A. Lee, Superconductivity in three-dimensional spin-orbit coupled semimetals, *Phys. Rev. B* **96**, 214514 (2017).
- [41] S. Kobayashi, A. Bhattacharya, C. Timm, and P. M. R. Brydon, Bogoliubov Fermi surfaces from pairing of emergent $j = \frac{3}{2}$ fermions on the pyrochlore lattice, *Phys. Rev. B* **105**, 134507 (2022).
- [42] C. Timm, A. P. Schnyder, D. F. Agterberg, and P. M. R. Brydon, Inflated nodes and surface states in superconducting half-Heusler compounds, *Phys. Rev. B* **96**, 094526 (2017).
- [43] R. A. Horn and C. R. Johnson, *Matrix Analysis* (Cambridge University Press, New York, 2012).
- [44] Wolfram Research, Inc., Mathematica, Version 13.0, Champaign, IL, 2021.
- [45] E. K. Dahl and A. Sudbø, Derivation of the Ginzburg-Landau equations for a ferromagnetic p -wave superconductor, *Phys. Rev. B* **75**, 144504 (2007).
- [46] M. Sigrist and K. Ueda, Phenomenological theory of unconventional superconductivity, *Rev. Mod. Phys.* **63**, 239 (1991).
- [47] P. Fulde and R. A. Ferrell, Superconductivity in a strong spin-exchange field, *Phys. Rev.* **135**, A550 (1964).